Programmable Triangulation Light Curtains: Supplementary Material

Jian Wang, Joseph Bartels, William Whittaker,
Aswin C. Sankaranarayanan, and Srinivasa G. Narasimhan

Carnegie Mellon University, Pittsburgh PA 15213, USA
{jianwan2,josephba,saswin}@andrew.cmu.edu,
{red}@cmu.edu, {srinivas}@cs.cmu.edu

1 General Triangulation Light Curtains

The main paper considers the case where rotation axes of the line camera and the line laser are parallel. Relaxing this to allow rotation about non-parallel lines or complete rotational freedom are mathematically interesting.

1.1 Rotation over two axes

When the line camera and line laser rotate over two axes, l_c and l_p, respectively, given a 3D path $\mathbf{p}(t)$, the generated ruled surface can be determined. Each line in the surface should not only go through $\mathbf{p}(t)$, but also be co-planar to l_c and l_p simultaneously.

We can write the parametric form of the generated light curtain $s(t,u) \subset \mathbb{R}^3$ as

$$s(t,u) = \mathbf{p}(t) + u\mathbf{r}(t),$$

where u is a scalar and $\mathbf{r}(t) \in \mathbb{R}^3$ is the direction of the line which is analyzed in the following from simple to general conditions.

- When $l_c \parallel l_p$ (see Fig. 1 (a.1)), the lines in light curtain should also be parallel to l_c or l_p, thus $\mathbf{r}(t)$ is a constant value and is l_c's direction.
- When l_c and l_p intersect at a point, denoted as $\mathbf{A}$ (see Fig. 1 (a.2)), the lines in light curtain should also go through $\mathbf{A}$, thus $\mathbf{r}(t) = \frac{\mathbf{p}(t)-\mathbf{A}}{\|\mathbf{p}(t)-\mathbf{A}\|_2}$.
- When l_c and l_p are non-coplanar (see Fig. 1 (a.3)), how to find $\mathbf{r}(t)$? We can form plane $\mathbf{p}(t)$-l_c first; if l_p intersects with this plane at $\mathbf{A}(t)$, the line should also pass $\mathbf{A}(t)$, thus $\mathbf{r}(t) = \frac{\mathbf{p}(t)-\mathbf{A}(t)}{\|\mathbf{p}(t)-\mathbf{A}(t)\|_2}$ (in the figure, we show examples at two t-s); if there is no intersection, meaning l_p is parallel to this plane, $\mathbf{r}(t)$ should be l_p's direction.

In Fig. 1(a), we set the 3D path $\mathbf{p}(t)$ to be the same which is a circle in xz-plane for three conditions, so that we can see how the light curtain changes when rotation axes change. When $l_c \parallel l_p \parallel y$-axis (a.1), light curtain is a cylinder. From (a.1) to (a.2), l_c and l_p rotate along z-axis reversely so that they intersect

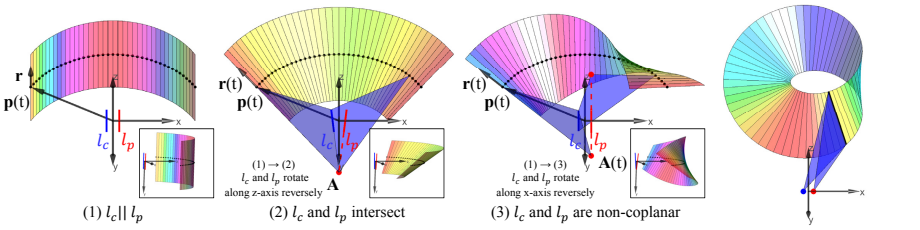

Fig. 1. General triangulation light curtains. (a) When each of the line camera and line laser rotates around an axis, the generated surfaces depend on the two rotation axes l_c and l_p and a given 3D path $\mathbf{p}(t)$: each line should go through $\mathbf{p}(t)$ and be co-planar to l_c and l_p. This requirement degenerates when $l_c \parallel l_p$ that each line be parallel to l_c (a.1), and when l_c and l_p intersect at a point that each line should also go through that point (a.2). In (a), the 3D path $\mathbf{p}(t)$ is intentionally set to be the same from (a.1) to (a.3); by comparing (a.1) with (a.2) and comparing (a.1) with (a.3), we can see how the light curtain changes when rotation axes change. (b) When each can rotate around a point, any ruled surface can be generated.

at a point in y-axis; the light curtain changes to a cone. From (a.1) to (a.3), l_c and l_p rotate along x-axis reversely; the light curtain skews.

Given a 3D path $\mathbf{p}(t)$, we next show how to compute the rotation angles of the line camera and line laser respectively. Without loss of generality, we assume that the origin of our coordinate system is at the midpoint between the centers of the line camera and line laser, the distance between two centers is b, directions of l_c and l_p are $\mathbf{M}$ and $\mathbf{N} \in \mathbb{R}^3$ respectively, and the given 3D path is at xz-plane and can be written as $\mathbf{p}(t) = [x(t), 0, z(t)]^\top$ (see Fig. 2 (a)). The rotation angle of the camera, which is measured counter-clockwise with respect to the xy-plane, is

$$\theta_c(t) = \text{angle}\left(\begin{bmatrix}0\\0\\1\end{bmatrix}, \begin{bmatrix}\mathbf{M}_x\\\mathbf{M}_y\\\mathbf{M}_z\end{bmatrix} \times \begin{bmatrix}x(t)+b/2\\0\\z(t)\end{bmatrix}\right) \tag{1}$$

and rotation angle of the laser is similar. They are

$$\begin{bmatrix}\theta_c(t)\\\theta_p(t)\end{bmatrix} = \begin{bmatrix}\arccos\left(\frac{-\mathbf{M}_y(x(t)+b/2)}{\sqrt{\mathbf{M}_y^2 z(t)^2+(\mathbf{M}_z x(t)+\mathbf{M}_z b/2-\mathbf{M}_x z(t))^2+(\mathbf{M}_y x(t)+\mathbf{M}_y b/2)^2}}\right)\\ \arccos\left(\frac{-\mathbf{N}_y(x(t)-b/2)}{\sqrt{\mathbf{N}_y^2 z(t)^2+(\mathbf{N}_z x(t)-\mathbf{N}_z b/2-\mathbf{N}_x z(t))^2+(\mathbf{N}_y x(t)-\mathbf{N}_y b/2)^2}}\right)\end{bmatrix}. \tag{2}$$

When l_c and l_p are co-planar, the equation can be simplified. Without loss of generality, we assume both are co-planar at xy-plane and are $\pm\gamma$ to y-axis (see Fig. 2(b) left),

$$\begin{bmatrix}\theta_c(t)\\\theta_p(t)\end{bmatrix} = \begin{bmatrix}\arccos\left(\frac{(x(t)+b/2)\cos\gamma}{\sqrt{(x(t)+b/2)^2\cos^2\gamma+z(t)^2}}\right)\\ \arccos\left(\frac{(x(t)-b/2)\cos\gamma}{\sqrt{(x(t)-b/2)^2\cos^2\gamma+z(t)^2}}\right)\end{bmatrix}, \tag{3}$$

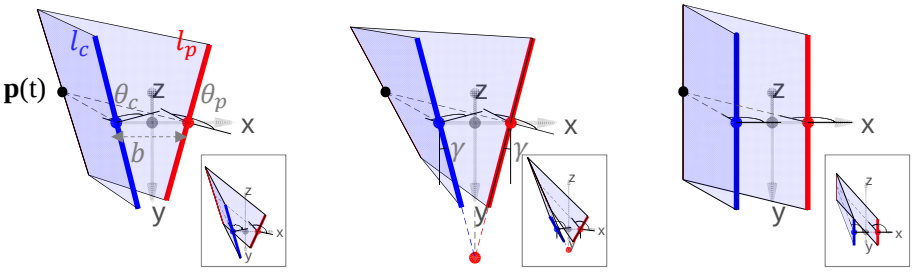

(a) General configuration (b) l_c and l_p are co-planar

Fig. 2. The coordinate frame for computing rotation angles of the camera and the laser given 3D path that the light curtain should pass. One point $\mathbf{p}(t)$ is drawn here. Insets are from different perspective.

and when $l_c \parallel l_p$ (Fig. 2 (b) right), $\gamma = 0$, this can be simplified further as

$$\begin{bmatrix}\theta_c(t)\\ \theta_p(t)\end{bmatrix} = \begin{bmatrix}\arccos\left(\frac{(x(t)+b/2)}{\sqrt{(x(t)+b/2)^2+z(t)^2}}\right)\\ \arccos\left(\frac{(x(t)-b/2)}{\sqrt{(x(t)-b/2)^2+z(t)^2}}\right)\end{bmatrix}. \tag{4}$$

1.2 Rotation over two points

When the line camera and line laser can rotate over two points respectively (full rotational degree of freedom), any ruled surface can be generated. Fig. 1(b) shows Möbius strip as an example. The proof is trivial, that any line in the ruled surface and the rotation center form a plane, which will determine the line camera or line laser's rotation.

2 Optimizing Triangulation Light Curtains

We add some proofs and discussion for Section 4 in the main paper here.

2.1 Derivation of thickness of light curtain

We draw Fig. 2(c) in the main paper again here as Fig. 3 with two variables introduced. α is the angle between camera line and laser line. a is the distance from laser's center to projection of the intersection onto baseline. The area of the quadrilateral shaded in Fig. 3 is

$$A = \frac{r_c\delta_c}{\sin\alpha}\frac{\Delta_L}{\sin\alpha}\sin\alpha = \frac{r_c\delta_c\Delta_L}{\sin\alpha}. \tag{5}$$

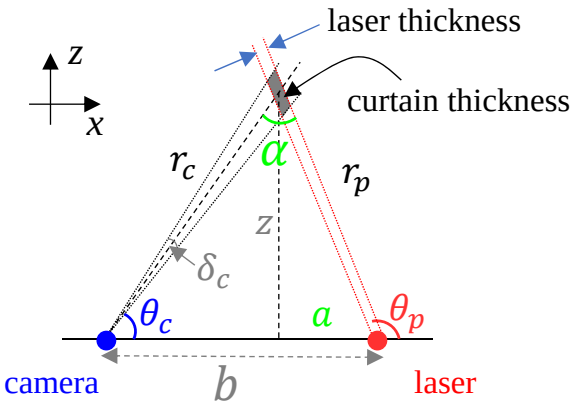

Fig. 3. Illustration of uncertainty and variables used.

We have $\sin\alpha = \sin(\theta_p - \theta_c) = \sin\theta_p\cos\theta_c - \sin\theta_c\cos\theta_p = \frac{z}{r_p}\frac{b-a}{r_c} - \frac{z}{r_c}\frac{-a}{r_p} = \frac{bz}{r_p r_c}$. Thus

$$A = \frac{r_c^2 r_p}{z}\frac{\delta_c \Delta_L}{b}. \tag{6}$$

2.2 Minimizing thickness and energy for nearby light curtains

When light curtain is far away, we can simply use largest possible baseline to minimize uncertainty, and no matter how we configure the device the consumed energy has no much difference. But when the light curtain is nearby, the best configuration is nontrivial.

Given the curtain shape in xz-plane $\mathbf{p}(\tau)$, the optimization problem **minimizing thickness** by triangulation can be formalized as following

$$\min_{C,P}\sum_{\tau=0}^{T} U(\tau) = \sum_{\tau=0}^{T}\frac{r_c(\tau)^2 r_p(\tau)}{|C-P|z(\tau)} \text{ s.t.} -\frac{b}{2} \leqslant C, P \leqslant \frac{b}{2} \tag{7}$$

where $r_c(\tau)$ and $r_p(\tau)$ are distances from $\mathbf{p}(\tau)$ to camera rotation center $[C,0,0]$ and laser rotation center $[P,0,0]$ respectively, $z(\tau)$ is depth of $\mathbf{p}(\tau)$, and $(-b/2, b/2)$ is the range that the rotation centers of the camera and laser can be positioned. For simplicity, we only consider cross section of light curtain in the xz-plane. In Fig. 4, first row under each curtain shows the optimization result. The best baseline is somewhere close to the full range and camera is closer to the center compared to laser because in the optimization r_c is squared and r_p is not.

When we want to **minimize energy**, the problem becomes

$$\min_{C,P}\sum_{\tau=0}^{T} E(\tau) = \sum_{\tau=0}^{T} r_p(\tau) r_c(\tau) \text{ s.t.} -\frac{b}{2} \leqslant C, P \leqslant \frac{b}{2} \tag{8}$$

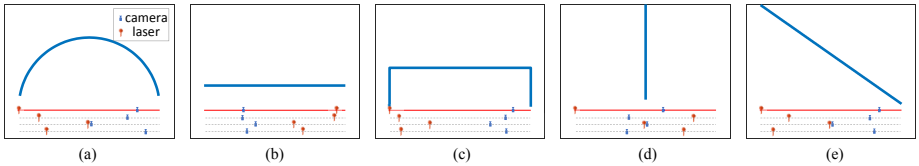

Fig. 4. Optimization of configuration of camera and laser for nearby light curtains. The dark blue line is the light curtain and red thin line under the curtain is the range that camera and laser can be placed. Four rows under each curtain indicate best configuration, blue dot for camera and red dot for laser, for four optimization problems respectively: minimize thickness only Eq. (7), minimize thickness subject to that energy smaller than a value Eq. (9), minimize energy only Eq. (8), and minimize energy subject to the thickness smaller than some value Eq. (10).

The result is shown in Fig. 4 third row under each curtain.

When we want to **minimize one subject to the other smaller than a pre-specified value**, like

$$\min_{C,P} \sum_{\tau=0}^{T} U(\tau) \;\text{ s.t.} \sum_{\tau=0}^{T} E(\tau) < e, \;\; -\frac{b}{2} \leqslant C, P \leqslant \frac{b}{2} \tag{9}$$

and

$$\min_{C,P} \sum_{\tau=0}^{T} E(\tau) \;\text{ s.t.} \sum_{\tau=0}^{T} U(\tau) < g, \;\; -\frac{b}{2} \leqslant C, P \leqslant \frac{b}{2} \tag{10}$$

the optimization result is difficult to predict. Fig. 4 second row and fourth row under each curtain show result of (9) and (10), respectively.

2.3 Combining with time-of-flight sensors

For a CW-TOF sensor, higher modulation frequency has better depth resolution. Suppose triangulation uncertainty is U, we can choose (i) modulation frequency f_m which satisfies $\frac{1}{2}c\frac{1}{f_m} = U$ where c is light speed, that is $f_m = 2U/c$, and (ii) delay in TOF so that the uncertainty zone by triangulation spans half phase, from 0 to π. This can be achieved by both 4-correlation TOF and 2-correlation TOF, as shown in Fig. 5. The resulted thickness becomes TOF's depth resolution. We showed results by a 2-correlation line TOF sensor in Fig. 8 in the main paper.

3 Calibration

Calibration is done by identifying the plane in the real world associated with each setting of laser's galvo and the line associated with each pair of camera's galvo and camera's pixel index.

To calibrate laser's galvo, we do the following:

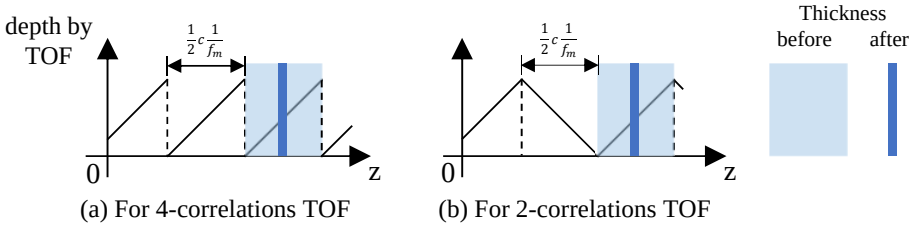

(a) For 4-correlations TOF (b) For 2-correlations TOF

Fig. 5. Combining with time-of-flight sensor to obtain thin light curtains.

- introduce a 2D helper camera whose intrinsic parameters are pre-calibrated [2];
- introduce a white planar board in the scene with fiducial markers at corners of a rectangle with known dimensions so that the board's plane equation can be known from the 2D helper camera;
- let the laser illuminate a line on the board which is observed by the 2D camera. 3D location of the dots in the line can be computed by intersection of 2D camera's ray and the board;
- move the board to another depth and get 3D location of another line;
- fit a plane based on these two lines, and repeat for the next galvo position.

To calibrate line camera's galvo, we do the following

- introduce a 2D helper projector;
- let the helper projector project horizontal and vertical gray code patterns to the same white board which are observed by the scanning line camera and 2D helper camera;
- do the decoding on gray coded images;
- find the correspondence between {galvo's position, line camera pixel} pair and helper camera's pixel; 3D location of the point corresponded to each {galvo's position, line camera pixel} pair can be known by the helper camera;
- move the board to another depth and get another point;
- fit a line based on two points for each pair.

In reality, we usually place the board at more than two depths to make the calibration more accurate.

4 Laser Safety

Laser safety, especially eye safety, puts a limit on the maximum energy that a laser system can emit to the scene, hence restricting the maximum working range. The laser's power density in W/m^2 at a distance smaller than Maximal Permissible Exposure (MPE) is considered eye safe. MPE is a function of laser wavelength, the subtended angle to the eye and duration [1].

Suppose our system scans the scene in the fashion that the laser is on for $100us$ and off for next $100us$, and waits for $500us$ for the mirror to rotate to

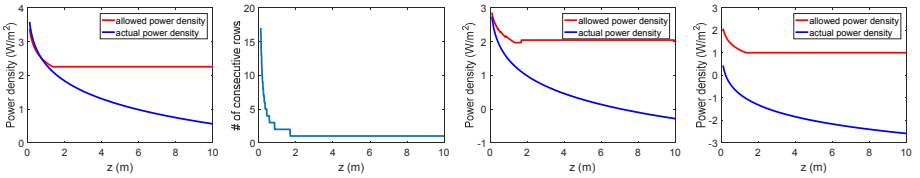

(a) Single pulse test (b) Consecutive rows test (c) Long time run (8 hrs) test

Fig. 6. Laser safety calculation. y-axis in the power density plots is in log-scale.

next position and repeat, these three conditions must be below MPE limit: (a) a single pulse with $100us$, (b) pulses of consecutive rows which illuminate the pupil for short depth, and (c) continuous operation over long period like a few hours for stationary eyes.

The specification of our laser is the following: peak power $700mW$, wavelength $638nm$, spot diameter $2mm$, fanout angle $\pi/4$ radians, thickness divergence angle 0.0021 radians (in Section 4 in the main paper thickness of laser is assumed to be constant for ease of derivation), and 200 line scans uniformly distributed in $\pi/4$'s angle of view. Duty cycle for single pulse is 1, and for one row is $100us/700us = 1/7$. The actual power density is computed as (duty cycle $\times$ peak power/illuminated area). Allowed power density MPE is calculated according to ANSI Z136.1 Table 5b in [1]. We plot MPE and actual power density in Fig. 6. It turns out requirement (a) gives the shortest safety distance which is $0.72m$ for our system. The power can be reduced depending on the application, for example, indoors we usually use 30% of the maximum power. If our red laser is replaced by a near-infrared or short-wave infrared laser, the safety distance is even shorter.

We can also use multiple line lasers. Although most of the time the light curtain is set to be several meters away, it must be guaranteed to be eye-safe at very close range (usually half meter or one meter away) and there is a huge gap between the usage distance and safety distance. By distributing power to multiple line lasers which intersect or "focus" at the same line in 3D, it can be eye-safe easily at close range as well as focused distance. In other words, the device is more eye-safe or higher total power can be used. Interference between multiple devices is also relieved by using this method.

5 Seeing through Scattering Media

Fig. 7(a) explains why light curtains see better than traditional imaging in scattering media. In traditional imaging, the camera receives light reflected from the object which is the signal of interest, as well as a single-bounce and multi-bounce global light from the medium. For the light curtain measurements, single-bounce backscattered light is optically blocked since the camera does not measure any light from the illumination plane except at the intersecting line; thus, a large

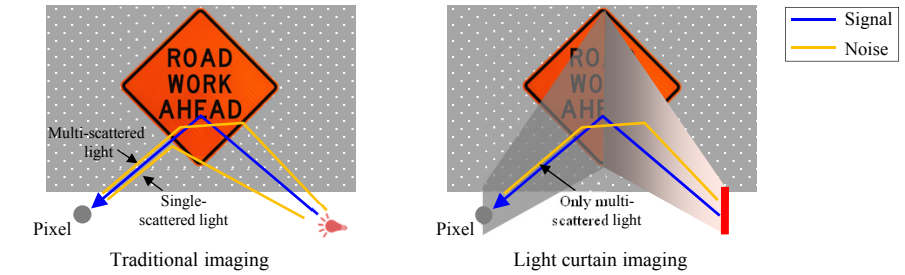

(a) Working principle

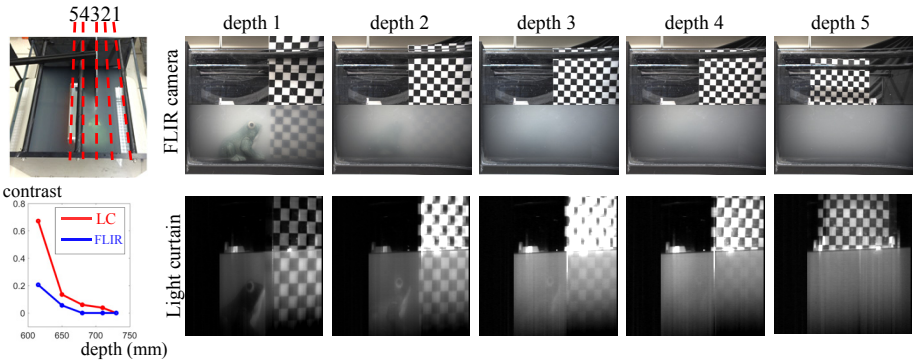

(i) Results on toy frog and checkboard

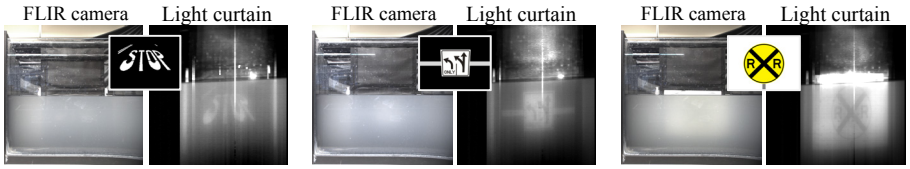

(ii) Results on printed road signs

(b) See through murky water

Fig. 7. Seeing through volumetric scattering medium. (a) Light curtain imaging has higher contrast than traditional imaging due to the block of single-scattered light which happens at medium particles. (b.i) The toy frog and checkerboard are placed in milky water at five different depths. We compare the images produced by a regular FLIR camera versus a light curtain at the same depth as the targets. Notice the better contrast on the light curtain result at various depths. Plot of contrast of the checkerboard part in the images is shown in the bottom left (LC in the plot legend refers to light curtain). (b.ii) More results on seeing some printed road signs.

portion of scattered light is removed and the contrast of the object at the intersection line is increased.

We placed a toy frog and a checkerboard within a tank filled with milky water and used our device with one fronto-parallel light curtain whose depth is set the same as the targets. We used a 2D visual camera under ceiling lights for comparison. We placed the targets at five depths and captured images. All raw images without any post-processing are shown in Fig. 7(b.i). Notice the better contrast of light curtain imaging over traditional imaging. We averaged pixel value of the white/black part in the checkerboard as I_W/I_B, respectively, and quantitatively computed the contrast of the checkerboard as $\frac{I_W - I_B}{I_W + I_B}$. The plot of the contrast of the images at five depths is shown in the bottom left, which indicates that our imaging improves the contrast significantly. In Fig. 7(b.ii) we show that while traditional imaging cannot see the printed road signs in the murky water, our imaging can.

References

1. American National Standards Institute: American national standard for safe use of lasers z136.1 (2014)
2. Bouguet, J.Y.: Matlab camera calibration toolbox. http://www.vision.caltech.edu/bouguetj/calib_doc/ (2000)